

## The Effects of Small-Scale Turbulence on Air–Sea Heat Flux

FABRICE VERON

*School of Marine Science and Policy, University of Delaware, Newark, Delaware*

W. KENDALL MELVILLE AND LUC LENAIN

*Scripps Institution of Oceanography, University of California, San Diego, La Jolla, California*

(Manuscript received 21 April 2010, in final form 24 August 2010)

### ABSTRACT

The air–sea exchange of heat is mainly controlled by the molecular diffusive layer adjacent to the surface. With an order of magnitude difference between the kinematic viscosity and thermal diffusivity of water, the thermal sublayer is embedded within its momentum analog: the viscous sublayer. Therefore, the surface heat exchange rates are greatly influenced by the surface kinematics and dynamics; in particular, small-scale phenomena, such as near-surface turbulence, have the greatest potential to affect the surface fluxes. Surface renewal theory was developed to parameterize the details of the turbulent transfer through the molecular sublayers. The theory assumes that turbulent eddies continuously replace surface water parcels with bulk fluid, which is not in equilibrium with the atmosphere and therefore is able to transfer heat. The so-called controlled-flux technique gives direct measurements of the mean surface lifetime of such surface renewal events. In this paper, the authors present results from field experiments, along with a review of surface renewal theory, and show that previous estimates of air–sea scalar fluxes using the controlled-flux technique may be erroneous if the probability density function (PDF) of surface renewal time scales is different from the routinely assumed exponential distribution. The authors show good agreement between measured and estimated heat fluxes using a surface renewal PDF that follows a  $\chi$  distribution. Finally, over the range of forcing conditions in these field experiments, a clear relationship between direct surface turbulence measurements and the mean surface renewal time scale is established. The relationship is not dependent on the turbulence generation mechanism. The authors suggest that direct surface turbulence measurements may lead to improved estimates of scalar air–sea fluxes.

### 1. Introduction

The air–sea fluxes of heat and momentum play a pivotal role in weather, global climate, and the general circulation of the ocean and atmosphere. Exchanges between the atmosphere and the ocean occur across the surface layers, and the rate at which they do is greatly influenced by the kinematics and dynamics of the boundary layers. This is particularly true for the transfer of heat that relies on exchange processes through the thermal molecular layer, which is usually located within the viscous sublayer. In recent years, there has been a renewed interest in trying to understand the processes that control these multiple air–sea fluxes. In particular, it has been found

that phenomena such as surface waves (especially breaking waves), turbulence on both sides of the interface, bubbles, droplets, and surfactants (among others) may influence the kinematics and dynamics of the surface and therefore play important roles in these fluxes.

The framework for our understanding of the momentum boundary layers in both the ocean and the atmosphere has come largely from the body of work resulting from extensive engineering studies of turbulent flows over rigid, flat surfaces, that is, wall-layer turbulence and the corresponding “law of the wall.” For air–sea interaction studies, efforts have focused on parameterizing air–sea fluxes with a mean flow speed, normally taken at 10-m height  $U_{10}$ . These bulk parameterizations rely on a drag coefficient for momentum flux and other bulk transfer coefficients for the scalar fluxes of heat, humidity, and gases, which are not constant but may depend on the wind speed and wave variables (see below). A significant improvement to the law-of-the-wall model was later

---

*Corresponding author address:* Fabrice Veron, 112C Robinson Hall, University of Delaware, School of Marine Science and Policy, College of Earth, Ocean and Environment, Newark, DE 19716.  
E-mail: fveron@udel.edu

obtained for the atmospheric boundary layer by including stratification effects parameterized by the so-called Monin–Obukhov length: the height at which shear and buoyant production of kinetic energy are equal. Monin–Obukhov similarity theory has been widely used and studied since the landmark Kansas experiment (Businger et al. 1971); over the past decades, the theory has been marginally improved (Panofsky and Dutton 1984).

However, the structure of the boundary layer over a rigid surface and that over a moving, fluid surface are quite different, and the processes that affect and control the air–sea fluxes are influenced by kinematics and dynamics of the boundary layer. Indeed, the role of the surface waves in the air–sea momentum flux has only been evaluated relatively recently (Hsu et al. 1981; Snyder et al. 1981; Rapp and Melville 1990; Komen et al. 1994). It is now accepted that ocean surface waves may support much of the momentum transfer from the atmosphere to the ocean. For example, following extensive studies of the role of waves on the air–sea momentum flux, the European Center for Medium-Range Weather Forecasting incorporated wave effects in their momentum flux estimates (Komen et al. 1994). More recently still, the influence of the surface waves on the momentum transfers have been examined in the context of wave growth (Hara and Belcher 2002), airflow separation (Kudryavtsev and Makin 2001; Donelan et al. 2004; Veron et al. 2007; Mueller and Veron 2009a), and production and transport of spray (Andreas 2004; Mueller and Veron 2009b). In addition, waves and wave breaking in particular have been shown to inject significant levels of turbulence in the surface layer and modify the energy balances that lead to the law of the wall (Agrawal et al. 1992; Thorpe 1993; Melville 1994; Anis and Moum 1995; Melville 1996; Drennan et al. 1996; Terray et al. 1996; Veron and Melville 1999; Melville et al. 2002; Thorpe et al. 2003; Gemmrich and Farmer 2004; Sullivan et al. 2004, 2007). The effect of waves on the fluxes of scalars is controversial at best, although recent evidence suggests that waves may play a direct role (Veron et al. 2008b) or perhaps have an indirect effect through the modulation of the turbulence and the consequent air–sea transfers (Sullivan and McWilliams 2002; Veron et al. 2009).

While the bulk formulae and Monin–Obukhov similarity theory led to significant progress in quantifying air–sea fluxes on larger scales, detailed studies of the smaller-scale surface phenomena such as Langmuir circulations and surface turbulence have generally been lacking, presumably because  $U_{10}$  is typically thought to be a good proxy for the dynamical state of the surface. However, an understanding of the actual kinematics and dynamics of small-scale turbulence (and the surface waves)

is especially relevant for the air–sea heat fluxes that occur through the ocean surface molecular, diffusive sub-layer, which is typically  $O(1)$  mm thick or less. This has become increasingly apparent in the studies of the sea surface temperature (SST) and “cool skin” bias (Wick et al. 1996; Castro et al. 2003; Ward and Donelan 2006; Ward 2006) with resulting parameterizations that specifically include the turbulence and waves. It has also become apparent in recent studies of air–sea gas transfer that point toward the need to incorporate the effects of small waves (Frew et al. 2004), wave breaking (Zappa et al. 2001), bubbles (Farmer et al. 1993), rain-induced turbulence (Ho et al. 2007), and Langmuir circulations (Veron and Melville 2001).

Studying the details of the kinematic and dynamic state of the surface is all the more difficult as scales associated with surface waves and turbulence overlap, leading to significant coupling and nonlinear interactions. However, recent advances in numerical models (Sullivan et al. 2000), theories (Teixeira and Belcher 2002), and experimental methods (Veron and Melville 2001; Veron et al. 2008a) allow us to start looking at this problem at time and spatial scales relevant for the scalar air–sea fluxes. In this paper, we present results of two field experiments on the kinematics of small-scale surface turbulence, its influence on the surface skin layer, and the resulting transfers of heat across the diffusive layer at the surface of the ocean. A variety of optical and electromechanical instruments are used to measure the evolution of the surface velocity and temperature fields (Veron et al. 2008a). We examine in particular the application of the controlled-flux technique (CFT), based on surface renewal theory, to remotely measure the air–sea heat flux.

## 2. Experiments and setup

Two field experiments were conducted from the Research Platform *FLIP*, moored off the coast of San Diego, California. The first took place from 21 to 29 July 2002 at 32°38.43'N, 117°57.42'W in 302 m of water. The second was from 20 to 26 August 2003 and took place west of Tanner Bank at 32°40.20'N, 119°19.46'W, in 312 m of water (Fig. 1).

The primary instruments included an active and passive infrared imaging and altimetry system (Veron et al. 2008a) and a direct eddy-covariance atmospheric flux package, including longwave and shortwave radiation measurements. The instruments were deployed at the end of the port boom of *FLIP* (Fig. 1) approximately 18 m from the hull at an elevation of 13 m MSL. Additional supporting data were obtained from two subsurface fast response thermistors (Branker TR-1040, 95 ms) placed at 1.2- and 2-m depth, and a waves ADCP (RDI Workhorse

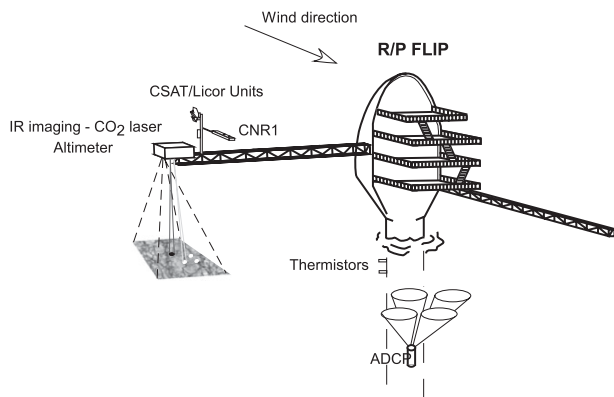


FIG. 1. Experimental setup on R/P *FLIP* during 20–26 Aug 2003.

600 kHz, at 15-m depth on the hull of *FLIP*), which yielded directional wave spectra and significant wave heights for the duration of the experiment. GPS position and *FLIP* heading were also sampled at 20 Hz.

The instrumentation is briefly described below and the detailed performance of the passive and active IR measurement system for measuring ocean surface kinematics can be found in Veron et al. (2008a).

#### a. Infrared imaging and altimetry system

The active and passive infrared imaging and altimetry system includes an infrared camera (Amber Galileo), a 60-W air-cooled CO<sub>2</sub> laser (Synrad Firestar T60) equipped with an industrial marking head (Synrad FH index) with two computer-controlled galvanometers, a laser altimeter (Riegl LD90–3100-EHS), a video camera (Pulnix TM-9701), a six-degrees-of-freedom motion package (Watson Gyro E604), and a single board computer (PC Pentium 4). All instruments were enclosed in a weatherproof air-conditioned aluminum housing. The computers and instruments were synchronized together to within 2 ms and to GPS time. The infrared camera was set to record temperature images (256 pixels × 256 pixels) at 60 Hz, with a 2-ms integration time, yielding better than 15-mK resolution. The video camera (768 pixels × 484 pixels) was synchronized to the infrared camera and acquired full frames at 30 Hz. The infrared CO<sub>2</sub> laser and accompanying marking head were used to actively lay down patterns of thermal “markers” on the ocean surface. This technique gives an estimate of the air–sea heat flux using the rate of decay of an imposed surface temperature perturbation (controlled-flux technique) (Jähne et al. 1989). The active heat markers were also used to perform thermal marking velocimetry (TMV) (Veron et al. 2008a), which yielded the Lagrangian velocity and other kinematic variables such as shear and vorticity, at the surface. Finally, the laser altimeter measured the distance to the water surface within both the infrared and

video images, at 12 kHz (averaged to 50 Hz) with a 5-cm diameter footprint. Infrared and video images were acquired for 20 min every hour with supporting data acquired continuously for the duration of the experiments. In this paper, to avoid sky reflectance and other effects, we present data from nighttime infrared imagery only.

#### b. Meteorological package

In addition to the optical infrared system, we used a meteorological package to acquire supporting meteorological and boundary layer flux data. It consisted of an eddy covariance system including a three-axis anemometer/thermometer (Campbell CSAT 3), an open path infrared hygrometer/CO<sub>2</sub> sensor (Licor 7500), a relative humidity/temperature sensor (Vaisala HMP45), and a net radiometer (CNR1). Turbulent fluxes of momentum, heat, and moisture were calculated over 30-min averages. The sonic temperature was corrected for humidity and pressure; rotation angles were obtained from the 30-min averages, and the latent heat flux was corrected for density variations (Webb et al. 1980). Also, the sonic velocity was corrected to account for platform motion using acceleration measurements from a Watson Gyro (E604) motion package. The eddy covariance system was not deployed during the first *FLIP* experiment in 2002.

Figure 2 shows a comparison between the fluxes measured with the eddy covariance system and those calculated with bulk formulae from the Tropical Ocean and Global Atmosphere Coupled Ocean–Atmosphere Response Experiment (TOGA COARE 3.0) algorithm (Fairall et al. 1996, 2003) for the whole duration of the August 2003 experiment. For the most part, the agreement is good, supporting the use of the Monin–Obukhov similarity theory for open ocean conditions (Edson et al. 2004); however, there are discrepancies that may be due to wave effects that are not included in the COARE 3.0 algorithm (Veron et al. 2008b). For the purposes of this paper, the generally good agreement gave us confidence that our covariance measurements were consistent with other measurements in the literature of the total flux above the diffusive and wave boundary layers.

### 3. Surface renewal theory and controlled-flux technique

Directly beneath the surface is a thin viscous sublayer where the exchange of momentum is governed in part by molecular viscous processes. With the difference between kinematic viscosity and thermal diffusivity being almost an order of magnitude, there is also an analogous thermal sublayer within the viscous sublayer. In the thermal sublayer, molecular processes dominate and control

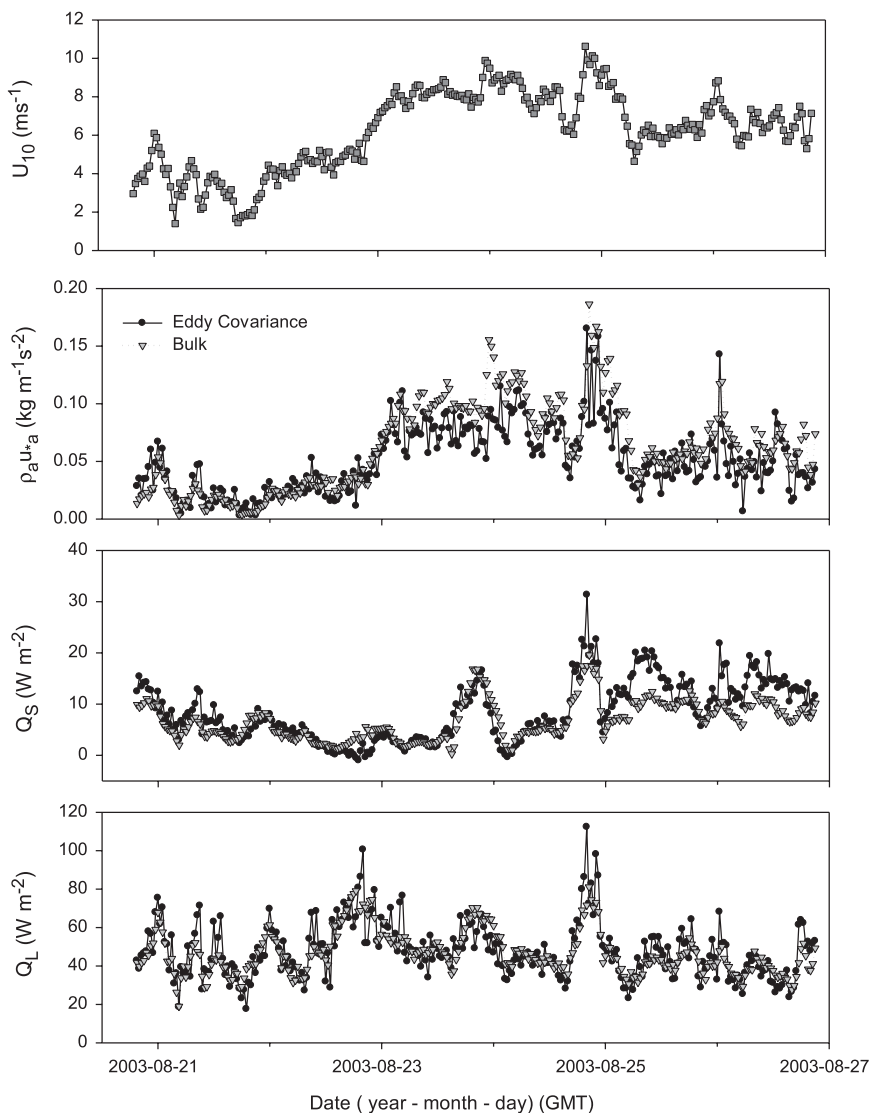


FIG. 2. Wind speed (equivalent 10 m), momentum, heat, and moisture fluxes measured by the eddy covariance system and compared with the TOGA COARE 3.0 bulk algorithm for the duration of the 2003 experiment.

the flux of heat across the layer (Ewing and McAlister 1960; McAlister 1964; Saunders 1967; Katsaros 1980; Paulson and Simpson 1981). At the air–sea interface, the thermal sublayer is typically  $O(0.1\text{--}1)$  mm since the net heat flux from the ocean to the atmosphere, that is, the sum of latent, sensible, and longwave radiation fluxes is generally positive upward, the surface temperature, or skin temperature  $T_{\text{skin}}$ , is typically a few tenths of a degree colder than the temperature at the base of the molecular layer  $T_{\text{subskin}}$ , the subskin sea temperature. The heat flux across the thermal molecular layer then matches the heat flux to the atmosphere and this leads to what is now referred to as the cool skin. This temperature difference,  $\Delta T_0 = T_{\text{skin}} - T_{\text{subskin}}$ , has received considerable

attention owing to its impact on the accuracy of remotely sensed SST (Schlüssel et al. 1990; Soloviev and Schlüssel 1994; Donlon et al. 1999; Wick et al. 1996; Castro et al. 2003; Wick et al. 2005). One can further assume a basic Fickian diffusion law, so, in the absence of downwelling shortwave radiation, the mean surface temperature difference  $\Delta T_0$  can then be related to the mean net flux of heat at the surface:

$$|\overline{Q}| = k_H \rho_w C_p |\Delta T_0|, \quad (1)$$

where the overbar denotes the average value,  $\rho_w$  is the water density,  $C_p$  the specific heat capacity of water, and  $k_H$  is the heat transfer velocity, which parameterizes the

details of the transfer mechanisms through the thermal sublayer. One such useful parameterization is that resulting from the surface renewal theory, which suggests that turbulent eddies continuously replace surface water parcels with water parcels from the bulk of the fluid, which are not in equilibrium with the atmosphere and therefore are available to transfer heat. Based on the work of Higbie (1935), Danckwerts (1951) extended the concept of surface renewal theory and also suggested that the renewal rate, the reciprocal of the surface lifetime  $\tau$  of a water parcel, could be described statistically by a probability density function (PDF)  $\Pi(\tau)$ , which he named the surface-age distribution function. Danckwerts further postulated that surface renewal lifetime should be exponentially distributed and  $\Pi(\tau) = \lambda e^{-\lambda\tau}$ , where  $\lambda$  is the mean renewal rate. Although Danckwerts's original paper deals with gas absorption and chemical reactions, if we apply his result [his Eq. (5)] to the heat problem, we find that

$$k_H = \sqrt{\kappa\lambda}, \quad (2)$$

where  $\kappa$  is the molecular diffusivity of heat. We will revisit this result below and further explore the details of how Eq. (2) was obtained.

The remaining challenge is the estimation or measurement of the renewal rate  $\lambda$ . Since the surface renewal is due to turbulent eddies, a natural choice for the surface renewal time is that associated with eddy turnover time at the Kolmogorov scale (Brutsaert 1975; Kitaigorodskii 1984). Later, the estimates of  $\lambda$  were refined for different wind speed regimes to include free and forced convection time scales, shear, and surface wave breaking (Soloviev and Schlüssel 1994; Clayson et al. 1996). For measurements, it became quickly apparent that infrared remote sensing would be the method of choice. Indeed, infrared radiometers typically operate at wavelengths for which the penetration depth is much smaller than both viscous and thermal molecular layers (McAlister 1964; McAlister and McLeish 1970; Downing and Williams 1975; Haußecker 1996). Passive methods have been quite successful and allow for visualization of the surface renewal processes from breaking and microbreaking waves (Jessup et al. 1997a,b; Zappa et al. 2001) and from shear and convective turbulence (Veron and Melville 2001; Garbe et al. 2004; Schimpf et al. 2004; Veron et al. 2008a). Direct measurements of the renewal rates usually require active infrared methods. The controlled flux technique (CFT) was first suggested by Jähne et al. (1989) and further refined by his group (Haußecker et al. 1995; Haußecker 1996; Jähne and Haußecker 1998; Haußecker et al. 2001). It has since been used in a number of other studies (Veron and Melville 2001; Zappa et al. 2001;

Asher et al. 2004; Atmane et al. 2004). The principle of the method is relatively simple. The surface of the water is locally heated using a CO<sub>2</sub> laser [with a wavelength of 10.6  $\mu\text{m}$  and a penetration depth  $h \sim O(10) \mu\text{m}$ , Downing and Williams (1975)]. This thermal marker on the water surface and its temperature time evolution can be tracked with a high-resolution thermal imager. Because the thermal molecular layer is embedded in the viscous layer, it is affected by the near-surface eddies serving as surface renewal events. Starting initially with the three-dimensional problem consistent with the finite horizontal extent of the temperature spot at the surface and neglecting any advection or shear effects due to surface currents, the diffusion equation including surface renewal becomes (Danckwerts 1951)

$$\frac{\partial \Delta T'(x, y, z, t)}{\partial t} = \kappa \nabla^2 (\Delta T'(x, y, z, t)) - \frac{1}{t_*} \Delta T'(x, y, z, t), \quad (3)$$

with  $\Delta T'(x, y, z, t) = T'(x, y, z, t) - T_{\text{subskin}}$ , that is, where we have subtracted a constant subskin temperature to the surface temperature  $T'(x, y, z, t)$ . Here  $t_*$  is the mean surface renewal time. Since the initial heat distribution generated by the CO<sub>2</sub> laser is Gaussian,  $\Delta T'(x, y, z, 0) = T_0 e^{-(x^2+y^2)/\sigma^2} e^{-z^2/h^2}$  in which  $\sigma$  is the size of the heat spot and is where the center of the temperature spot is at  $(x, y) = (0, 0)$ . Integrating in  $(x, y)$  over an area containing the temperature spot and its finite gradients, the three-dimensional equation above reduces to

$$\frac{\partial \Delta T(z, t)}{\partial t} = \kappa \frac{\partial^2 \Delta T(z, t)}{\partial z^2} - \frac{1}{t_*} \Delta T(z, t), \quad (4)$$

where  $T(z, t) = \iint T'(x, y, z, t) dx dy$ . A simple solution to Eq. (4) for the spot temperature (at the surface) can then be obtained:

$$T(0, t) = T_0 \frac{h}{\sqrt{h^2 + 4\kappa t}} e^{-t/t_*} + T_{\text{subskin}}. \quad (5)$$

By tracking the temperature decay of the locally heated spots at the water surface, the mean surface renewal time  $t_*$  can then be directly measured. In the case of the exponential PDF put forth by Danckwerts (1951), the mean surface renewal time  $t_*$  is

$$\begin{aligned} t_* &= \int_0^\infty \tau \Pi(\tau) d\tau \\ &= \tau \lambda e^{-\lambda\tau} d\tau \\ &= \lambda^{-1}, \end{aligned} \quad (6)$$

where  $\lambda$  is the surface renewal rate associated with the exponential PDF.

In summary, the Fickian diffusion law, Eq. (1), gives the relationship between the heat flux and the temperature gradient across the diffusive layer where the transfer velocity,  $k_H$ , incorporates the details of the (turbulent) transfer mechanisms. Surface renewal theory finds a simple relationship between the transfer velocity and renewal rate, Eq. (2), and finally the CFT allows for direct measurements of the renewal rate as described above, Eqs. (5) and (6).

For what follows, it is convenient to formally derive the details of how Danckwerts arrived at Eq. (2). Across the molecular layer, the temperature is described with a simple diffusion model. Again, we neglect any advection or shear effects due to surface currents, consider the horizontally integrated temperature, and subtract a constant subskin temperature to obtain the temperature difference  $\Delta T = T(z, t) - T_{\text{subskin}}$ . In addition, if we assume that the temperature is uniform with depth at  $t = 0$ , the governing equation then reduces to Eq. (4) without the surface renewal term:

$$\frac{\partial \Delta T(z, t)}{\partial t} = \kappa \frac{\partial^2 \Delta T(z, t)}{\partial z^2} \quad (7a)$$

with the initial and boundary conditions

$$\Delta T(z, t) = 0 \quad \text{for } t \leq 0, \quad (7b)$$

$$\Delta T(z, t) \rightarrow 0 \quad \text{as } z \rightarrow -\infty, \quad \text{and} \quad (7c)$$

$$\Omega(\Delta T(z, t)) = 0 \quad \text{at } z = 0. \quad (7d)$$

The last equation above,  $\Omega(\Delta T(z, t)) = 0$ , represents the surface boundary condition. Typical surface boundary conditions are either a Dirichlet condition where the temperature difference is constant or a Neumann condition where the gradient, that is, the flux through the surface, is fixed. Let us keep the surface boundary condition as general as possible for now and use

$$-\kappa \rho_w C_p \frac{\partial \Delta T(z, t)}{\partial z} = Q(t) \quad \text{at } z = 0, \quad (8)$$

where  $Q(t)$  is the upward time-dependent heat flux at the surface. We consider here a general form for the heat flux and describe its time dependence as a sum of powers of time  $t$ :

$$Q(t) = \sum_i \alpha_i t^i, \quad (9)$$

where  $i$  can be any real number such that  $i > -1$  and  $\alpha_i$  the corresponding weighting coefficient of  $t^i$ . This does retain generality in the surface condition, and we shall

see below that, obviously,  $i = 0$  is the Neumann condition and  $i = -1/2$  corresponds to the Dirichlet condition. Using Laplace transform techniques to solve the system of equations, (7) and (8), a general solution for the time and space dependence of the temperature deviation is given by (Veron and Melville 2001):

$$\begin{aligned} \Delta T(z, t) = & -\alpha_i \Gamma(i+1) \frac{1}{\rho_w C_p \sqrt{\kappa \pi}} \\ & \times 2^{i+1} t^{(i+1/2)} e^{-z^2/(8\kappa t)} D_{-2(i+1)}(\sqrt{z^2/(8\kappa t)}), \end{aligned} \quad (10)$$

where  $D$  is the parabolic cylinder function. In particular, the relationship between the surface temperature difference,  $\Delta T_0(t) = \Delta T(z = 0, t)$ , and the flux  $Q(t)$  is given by

$$\begin{aligned} \Delta T_0(t) = & -\frac{\Gamma(i+1)}{\Gamma(i+3/2)} \frac{\alpha_i}{\rho_w C_p \sqrt{\kappa}} t^{(i+1/2)} \\ = & -\frac{\Gamma(i+1)}{\Gamma(i+3/2)} \frac{Q(t) \sqrt{t}}{\rho_w C_p \sqrt{\kappa}}. \end{aligned} \quad (11)$$

When  $i = -1/2$ ,

$$\Delta T_0 = -\frac{Q(t) \sqrt{\pi t}}{\rho_w C_p \sqrt{\kappa}}, \quad (12)$$

and the temperature difference across the thermal layer,  $\Delta T_0$ , is constant, while the surface heat flux  $Q(t)$  is time dependent. This is the Dirichlet boundary condition and the temperature profile of Eq. (10) then reduces to the well-known complementary error function solution,

$$\begin{aligned} \Delta T(z, t) = & \Delta T_0 \operatorname{erfc}\left(\frac{-z}{2\sqrt{\kappa t}}\right) \\ = & -\frac{Q(t) \sqrt{\pi t}}{\rho_w C_p \sqrt{\kappa}} \operatorname{erfc}\left(\frac{-z}{2\sqrt{\kappa t}}\right). \end{aligned} \quad (13)$$

Figure 3a shows examples of the solution for  $\Delta T(z, t)$  with a Dirichlet surface boundary condition, where  $\Delta T_0$  is constant and the variable surface heat flux was chosen as  $Q(t) = 150t^{-1/2} \text{ W m}^{-2}$ . The thermal boundary layer grows with time as heat diffuses downward. Using Eq. (12) to obtain the instantaneous time-dependent surface heat flux,

$$Q(t) = -\frac{\Delta T_0 \rho_w C_p \sqrt{\kappa}}{\sqrt{\pi t}}, \quad (14)$$

and going back to the surface renewal ideas put forth by Higbie (1935) and Danckwerts (1951) where surface

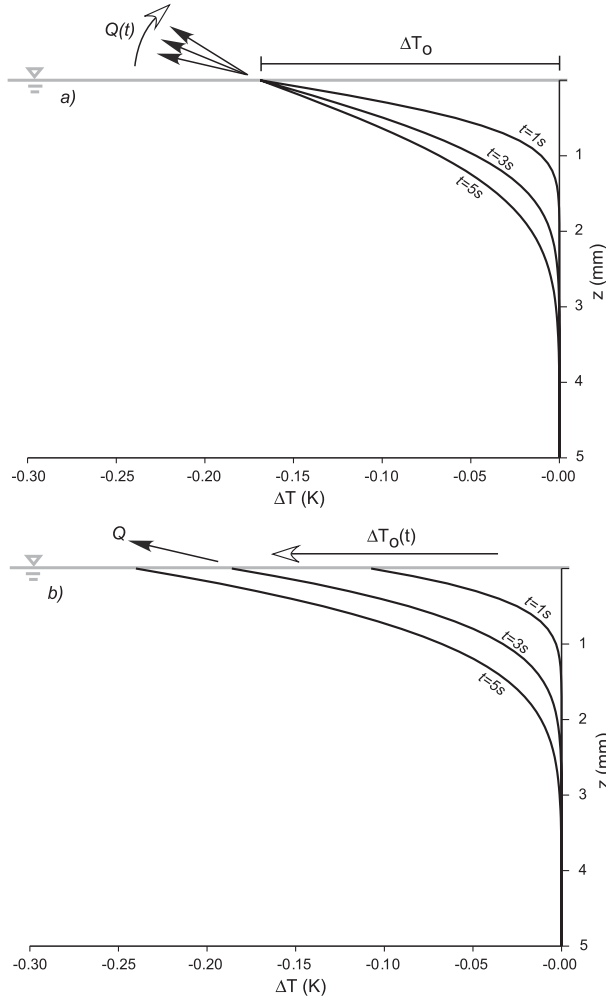


FIG. 3. Example for  $\Delta T(z, t)$  with the two boundary conditions described in the text: (a) Dirichlet, a constant temperature difference and a variable surface flux (slope of the temperature profile at the surface), and (b) Neumann, a constant surface flux leading to an increasing skin – subskin temperature difference.

renewal times are given by a probability density function  $\Pi(t)$ , the mean heat flux is then given by (Danckwerts 1951; Asher et al. 2004)

$$\bar{Q} = - \int_0^\infty \frac{\Delta T_0 \rho_w C_p \sqrt{\kappa}}{\sqrt{\pi \tau}} \Pi(\tau) d\tau. \quad (15)$$

Furthermore, when the surface renewal rate is given by an exponential PDF, the average surface flux and the skin – subskin temperature difference are related by

$$\bar{Q} = -\Delta T_0 \rho_w C_p \sqrt{\kappa \lambda}. \quad (16)$$

This is the result found by Danckwerts (1951), his Eqs. (1) and (2). From Eqs. (1) and (16), we fall back on Eq. (2)

and find that  $|k_H| = \sqrt{\kappa \lambda}$ , which is the formula used in all CFT studies to date (Haußecker et al. 1995; Haußecker 1996; Jähne and Haußecker 1998; Veron and Melville 2001; Zappa et al. 2001; Asher et al. 2004; Atmane et al. 2004). However, this was obtained on the basis of a Dirichlet boundary condition, which is indeed appropriate for waterside limited gas concentration where most of the resistance to the gas flux is provided by the aqueous boundary layer, which in turn supports the main gas concentration difference. For the temperature however, it is unclear that a Dirichlet boundary condition is appropriate. Indeed, the total net heat flux (in these conditions at night) is the sum of sensible, latent, and longwave radiation fluxes, with the latter two being typically much larger than the sensible heat flux. On that basis, Soloviev and Schlüssel (1994) argued that temperature deviations and the possible local reduction of  $\partial \Delta T(z, t) / \partial z|_{z=0}$  [Eq. (8)] induced by surface renewal events lead to a negligible deviation in the total heat flux. They therefore concluded that a constant-flux (Neumann) boundary condition is appropriate. Moreover, although turbulent eddies in the atmosphere can alter the surface condition for the (air-side limited) water vapor gradient near the interface, the time scale associated with the atmospheric surface renewal is much smaller than that in the water. Therefore, in the statistical context considered here, it seems appropriate to consider the surface heat flux to be constant. Then, in the case where  $i = 0$ , Eq. (11) now leads to

$$\Delta T_0(t) = - \frac{2Q\sqrt{t}}{\rho_w C_p \sqrt{\pi \kappa}}, \quad (17)$$

where the surface flux  $Q$  is constant and the temperature difference across the thermal layer  $\Delta T_0$  is time dependent. The temperature profile given in Eq. (10) then reduces to

$$\begin{aligned} \Delta T(z, t) &= \Delta T_0(t) \left\{ e^{-z^2/(4\kappa t)} + \frac{z\sqrt{\pi}}{2\sqrt{\kappa t}} \operatorname{erfc}[-z/(2\sqrt{\kappa t})] \right\} \\ &= - \frac{Q\sqrt{\kappa}}{\rho_w C_p \kappa} \left\{ \frac{2\sqrt{t}}{\sqrt{\pi}} e^{-z^2/(4\kappa t)} + \frac{z}{\sqrt{\kappa}} \operatorname{erfc}[-z/(2\sqrt{\kappa t})] \right\}. \end{aligned} \quad (18)$$

Figure 3b shows examples of the solution  $\Delta T(z, t)$  to the heat diffusion equation with a Neumann surface boundary condition where the surface heat flux is constant and chosen as  $Q = 150 \text{ W m}^{-2}$ . Again, the thermal boundary layer grows with time as heat diffuses downward. Once more, assuming that the surface renewal times are given by a probability density function  $\Pi(t)$ , we find from Eq. (17) the mean temperature difference at the surface,

$$\overline{\Delta T_0} = - \int_0^\infty \frac{2Q\sqrt{\tau}}{\rho_w C_p \sqrt{\pi\kappa}} \Pi(\tau) d\tau. \quad (19)$$

Again, when the surface renewal rate is given by an exponential PDF, the relationship between the heat flux  $Q$  and the skin – subskin temperature difference  $\Delta T_0$  is

$$\overline{\Delta T_0} = - \frac{Q}{\rho_w C_p \sqrt{\kappa\lambda}}. \quad (20)$$

In the case where the surface renewal rate is given by an exponential PDF, Eq. (20) happens to be identical to Eq. (16). However, other surface-age distributions lead to different results.

The analysis presented above suggests that, when heat is used as a proxy marker for CFT studies, Eq. (19) should be used in place of Eq. (15) because it uses the correct surface boundary condition for heat. Also, if the surface renewal times are given by a PDF other than exponential, Eq. (19) yields a different formula than that used to date. This suggests that results obtained using Eq. (15) [or Eq. (16)] might be questionable. This is a possible explanation for the discrepancies between some CFT-estimated and direct heat flux measurements (Asher et al. 2004). This may also explain the inconsistencies between simultaneous estimates of heat and gas fluxes using CFT (Atmane et al. 2004) since the assumed boundary condition in these studies is correct for gas flux but not for heat flux. Furthermore, other probability density functions for the surface renewal times have been proposed (Asher and Pankow 1989; Garbe et al. 2004; Atmane et al. 2004) with some degree of success. We present below estimates of the surface heat flux using the CFT technique in conjunction with other infrared imagery techniques.

## 4. Experimental results

### a. Combined passive and active infrared imagery

We have developed a passive and active infrared imagery and altimetry package designed to study the small-scale surface turbulence, surface waves, and other small-scale air–sea interaction processes. The instrumentation is described in detail in Veron et al. (2008a). Every even minute, passive infrared images of the ocean surface are acquired at a rate of 60 Hz for a minute. In the cases presented here, the spatial resolution was approximately 0.8 cm but varies slightly with the altitude change due to the presence of surface waves. We have systematically corrected for this effect using the instantaneous distance from the infrared camera to the instantaneous water surface measured with the altimeter. Each temperature image

therefore has its own spatial resolution, which is used to calculate accurate surface displacements with both the passive [using particle image velocimetry (PIV) techniques] and the active marking methods (TMV). During odd minutes, a 60-W air-cooled CO<sub>2</sub> laser is used to actively mark the surface with a pattern of seven heat spots used as passive Lagrangian markers. The full pattern is generated on the surface at a rate of 0.5 Hz. Each spot is approximately 3.5 cm in diameter initially. The temperature rise associated with individual spots was kept below 2 K so that buoyancy effects can be neglected. The heat markers were laid down by firing the laser for approximately 10 ms at full power. The “writing” speed and the speed of the galvanometers controlling the scanning mirrors allowed us to lay down an array of seven spots in 70 ms, corresponding to five to six IR temperature images. These spots are then tracked, and the pattern displacement and distortion gives a measure of the surface drift and velocity gradients, respectively. Furthermore, the temperature decay of the spots gives an estimate of the mean surface renewal rate, Eq. (5).

Figure 4 shows examples of ocean surface infrared images collected from R/P *FLIP* in August 2003 under various wind speed conditions. The image footprints are approximately 2 m × 2 m. The equivalent 10-m neutral wind speeds are 0.5, 3, and 6.5 m s<sup>-1</sup>. The grayscale is arbitrary and represents the temperature where black is cold and white is hot. Convection patterns at the lowest wind speed are clearly visible. In general, a transitional regime at approximately 1 m s<sup>-1</sup> can be observed. As the wind speed increases, the turbulence also increases, homogenizing the temperature signal at the surface, resulting in a loss of contrast or reduced variance in the temperature images. Also, the heat markers and the distortion of the initial pattern are clearly visible. It is also evident that the rate of temperature decay increases with increasing wind speed, indicating increased turbulence and surface renewal rates (see below). The image pairs (separated by 665 ms) show how the pattern is displaced, rotated, dilated, and sheared by the surface velocity field.

From the passive images, we derive statistics of the surface temperature deviations. Similar to the methods described in Schimpf et al. (2004) and Garbe et al. (2004), we estimate PDFs of the surface temperature deviation (i.e., the local instantaneous surface temperature minus the skin temperature, where the skin temperature is defined as the image mean surface temperature). From there, we estimate the skin – subskin temperature difference as the 99th percentile of the temperature deviation PDF (see Veron et al. 2008a). In other words, we assume that we capture the renewal event in a statistically significant manner over the footprint of the infrared

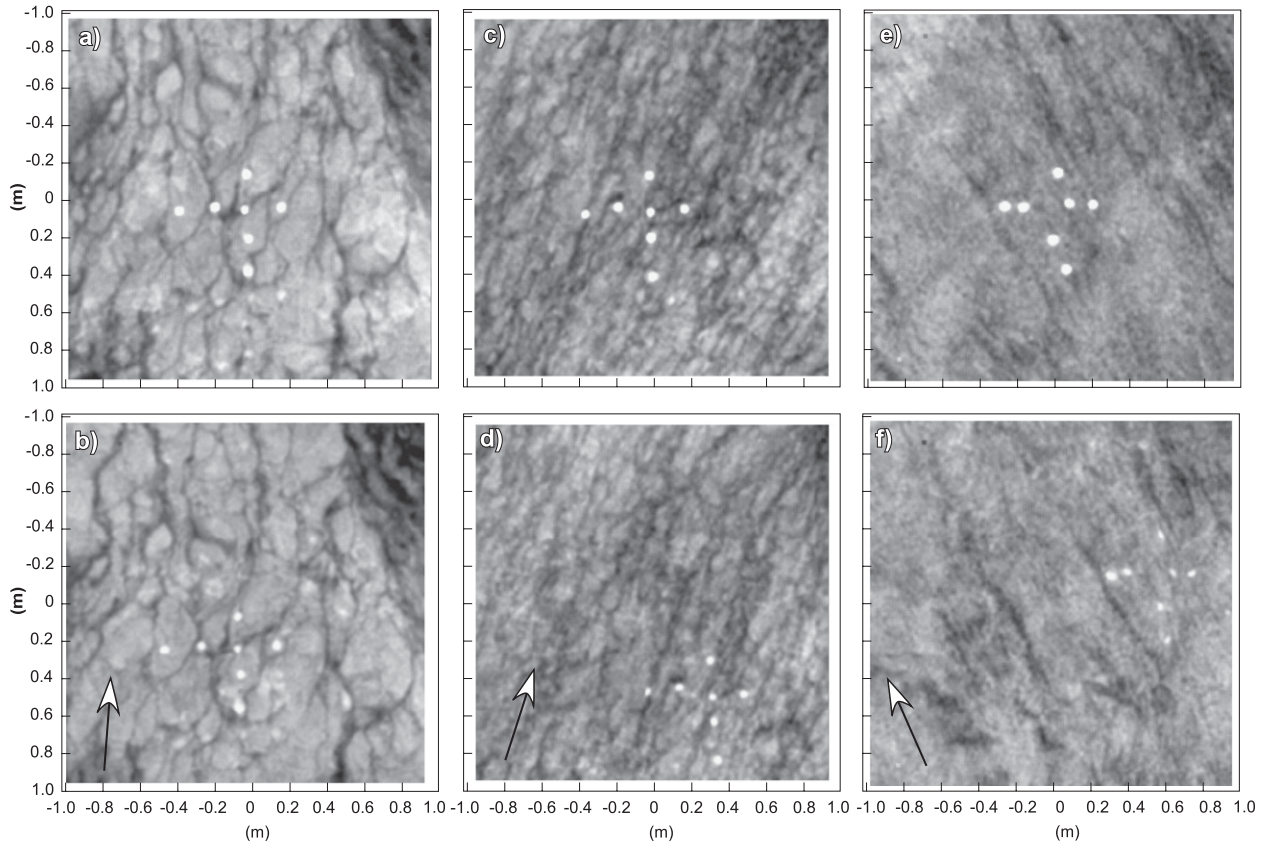


FIG. 4. Pairs of SST images taken 0.665 s apart. The images show the Lagrangian heat markers (lighter spots) and are taken for wind speeds of (a),(b)  $0.5 \text{ m s}^{-1}$ ; (c),(d)  $3 \text{ m s}^{-1}$ ; and (e),(f)  $6.5 \text{ m s}^{-1}$ . The arrow shows the wind direction. Note how the active TMV pattern fades with time and is displaced, rotated, dilated, and sheared by the surface velocity field. Note also the development of linear temperature structures at the higher wind speeds.

camera and the sampling time (20 min). Then the mean (temporal and spatial) of the temperature images represents the skin temperature, and the 99th percentile warmest temperature detected is therefore that of the subskin fluid, that is, that of a parcel of water that has just been transported to the surface by a renewal event. Figure 5 shows the 20-min average of the skin – subskin temperature difference as a function of wind speed. The results are consistent with previous estimates (Wick et al. 1992, 1996; Donlon and Robinson 1997; Donlon et al. 1999, 2002; Wick et al. 2005; Ward 2006), albeit on the lower end of the range reported, which is likely a result of the depth,  $O(1)$  m, at which these bulk (i.e., deeper than our subskin estimate) temperature measurements are typically made. With increasing wind speeds,  $\Delta T_0$  decreases as molecular and convective heat transfer diminishes and the role of shear-generated turbulent heat transfer gradually increases, with the transition from free to forced convection (Donlon et al. 1999).

This increase in surface turbulence activity can also be seen in the data from the active infrared technique.

Figure 6 shows the time series of the normalized active marker temperatures for various wind speeds. The temperature decay curve is obtained from averaging individual decay curves from the active pattern (7 spots) and over a minute of data (30 markings). It shows that the temperature time decay agrees remarkably well with the theoretical function given by Eq. (5) (see inset). Furthermore, the decay rate increases with wind speed, indicating that the mean time interval between consecutive surface renewal events becomes shorter with increased wind forcing. Indeed, Fig. 7 shows the mean renewal time  $t_*$  as a function of wind speed and airside friction velocity and a decrease with increasing wind forcing. It also shows that  $t_* \sim U_{10}^{-7/4}$  and  $t_* \sim u_{*a}^{-3/2}$  for  $4 \text{ m s}^{-1} < U_{10} < 10 \text{ m s}^{-1}$ , indicating that  $u_{*a} \sim U_{10}^{7/6}$  in this regime. This also indicates, at least for this regime, that the drag coefficient is a weak function of the wind speed  $C_D \sim U_{10}^{1/3}$ , which is in agreement with accepted parameterizations of the drag coefficient (Fairall et al. 1996, 2003).

At wind speeds where  $U_{10} < 4 \text{ m s}^{-1}$ , the surface renewal time scale departs from these trends and remains

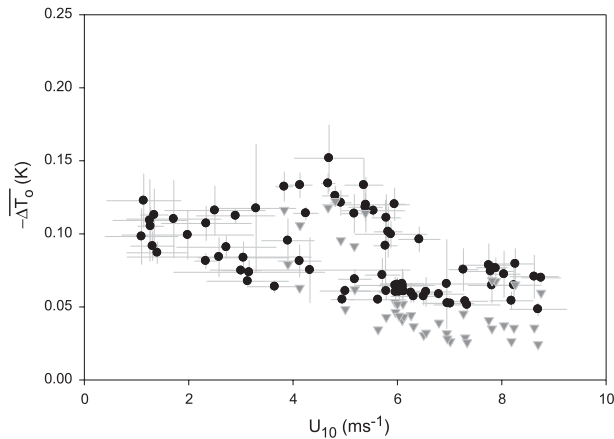


FIG. 5. Measured skin – subskin temperature difference as a function of wind speed. For reference, we also show (gray triangles) estimates of the skin – subskin temperature difference using Saunders formula (Saunders 1967) with  $\lambda = 2.4$  (Ward and Donelan 2006).

relatively low, albeit with some scatter in the data. This likely indicates that, as suggested by Soloviev and Schlüssel (1994) and Wick (1995), the low wind speed regime might be dominated by free convection. We note that this transition in the data also corresponds to the transition from smooth to rough flow (Kraus and Businger 1994); however, there is no reason to anticipate that the turbulence would remain relatively high (i.e., the renewal time scale would remain low) in the smooth flow limit. These results are also consistent with our previous measurements of surface turbulence statistics showing that, in the field, surface turbulence remains, even at very low wind speeds (Veron et al. 2008a).

If shear turbulence were to account for the surface renewal events for wind speeds  $U_{10} > 4 \text{ m s}^{-1}$ , the surface renewal time scale, as first suggested by Brutsaert (1975), should be equivalent to the Kolmogorov time scale; that is,  $t_k = (\nu_w/\epsilon)^{1/2}$  in which  $\nu_w$  is the kinematic viscosity of water and  $\epsilon$  is the turbulent kinetic energy dissipation. This form of the surface renewal time scale, which assumes that there is a balance between dissipation and production of turbulence by the mean shear flow, was adopted in the landmark paper by Liu, Katsaros, and Businger (1979). Later, equivalent parameterizations were developed by Soloviev and Schlüssel (1994) and Wick (1995) who, in addition, considered the effect of free convection at low wind speeds. Here

$$t_k = \left( \frac{u_{*w}^2 \partial \bar{U} / \partial z}{\nu_w} \right)^{-1/2} \sim \left( \frac{u_{*w}^2 U_0}{\nu_w H} \right)^{-1/2}, \quad (21)$$

where  $U_0$  and  $u_{*w}$  are the surface drift velocity and the waterside friction velocity, respectively, and where the

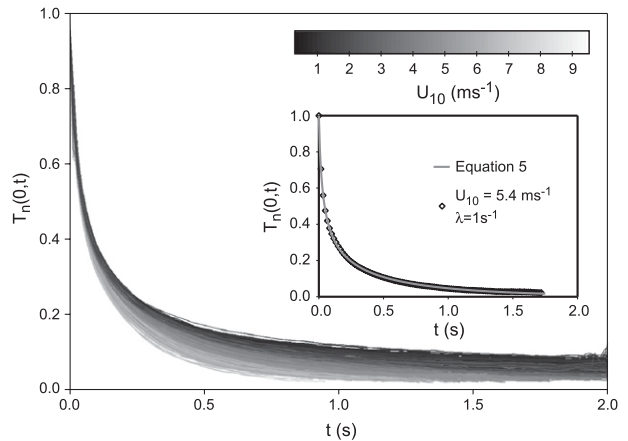


FIG. 6. Normalized surface temperature evolution of the active heat markers laid down on the surface by the CO<sub>2</sub> laser for different wind speeds ranging from 0.5 to 8.8  $\text{m s}^{-1}$ . The inset shows a single curve (diamonds) obtained from averaging all available individual spot temperatures  $T_n(0, t)$  for 1 min at  $U_{10} = 5.4 \text{ m s}^{-1}$ . The gray curve is the theoretical prediction from Eq. (5).

shear is estimated with outer scales with  $H$  a length scale therefore associated with the shear boundary layer. If we choose to parameterize surface renewal in this manner and assume that our measured  $t_* \sim t_k$ , and since  $\rho_a u_{*a}^2 = \rho_w u_{*w}^2$ , we find that  $H^{1/2} \sim U_0^{1/2} u_{*w}^{-1/2} \sim U_0^{1/2} u_{*a}^{-1/2}$ . Considering that the surface drift is a fraction of the atmospheric 10-m wind speed  $U_0 \sim O(10^{-2})U_{10}$ , we find that  $H \sim C_D^{-1/2} \sim U_{10}^{-1/6}$  and  $H$  is nearly constant for  $U_{10} > 4 \text{ m s}^{-1}$ . This indicates that the length scale associated with the waterside shear layer subjected to surface renewal events becomes smaller with increasing wind speed, albeit quite weakly. If we then define a Reynolds number based on these outer scales (i.e.,  $U_0$  and  $H$ ),

$$\text{Re} = \frac{U_0 H}{\nu_w}, \quad (22)$$

we find that the scaling of the renewal time scale with inner variables (i.e.,  $u_{*w}$ ) depends weakly on the Reynolds number:

$$t_* \frac{u_{*w}^2}{\nu_w} \sim \text{Re}^{7/10}. \quad (23)$$

This is consistent with the results of Kim et al. (1971) and Luchik and Tiederman (1987), who found dependences of  $\text{Re}^{0.76}$  and  $\text{Re}^{0.73}$ , respectively, for the time scales associated with turbulent bursts ejected from a solid boundary. We also note that  $t_r \sim \nu_w/u_{*w}^2$  is the surface renewal time scale used by Soloviev and Schlüssel (1994) for moderate wind speeds. In a sense, this approach differs from their parameterization only in that

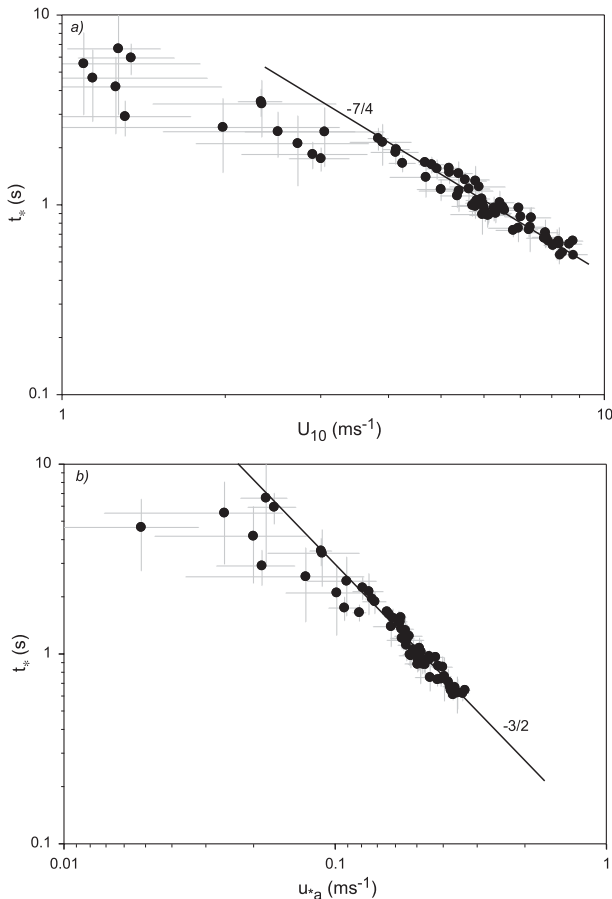


FIG. 7. (a) Mean surface renewal time  $t_*$  as a function of wind speed. The solid line shows a  $-7/4$  slope. (b) The mean surface renewal time as a function of airside friction velocity, exhibiting a  $-3/2$  dependence at higher friction velocities.

they did not account for a (relatively weak) Reynolds number dependence. Future parameterizations of surface renewal time scales might seek to incorporate a Reynolds number dependence as well. We note, however, that, besides the difficulty of finding an appropriate length scale  $H$ , this approach does not account for the presence of a deformable boundary, the presence of (breaking) waves, and other free-surface mechanisms that generate turbulence (e.g., Langmuir circulations).

At the lower wind speeds, shear alone would generate relatively weak turbulence and large  $t_*$  while the observed renewal time scales of Fig. 7 remains less than 10 s, indicating that, even at very low wind speeds, turbulence is nonetheless still present and disrupts the surface molecular layers with some intensity. This indicates that sources other than shear production are at play and further enhance the generation of turbulence. In fact, at the lower wind speeds, the surface renewal times are likely to scale with the convective time scale (Clayson

et al. 1996; Wick et al. 1996). However, this time scale depends on the surface heat flux, which is not known a priori, especially if one hopes to use these infrared techniques to remotely measure heat flux.

At higher wind speeds, shear-generated turbulence alone, as previously remarked, does not account for the turbulence generated by breaking surface waves and Langmuir circulations, which can represent a significant fraction of the total turbulence generation in all but the most benign conditions (Melville 1996; Melville et al. 1998; Veron and Melville 2001). Therefore, the apparent transition around  $U_{10} \approx 4 \text{ m s}^{-1}$  seen on Fig. 7, be it from smooth to rough flow, free to forced convection, or a combination thereof, and the presence of breaking waves, Langmuir circulations, and other turbulence generating phenomena, prevent the use of wind speed or wind stress as a universal predictor of the surface renewal time scale over a large range of conditions.

To remedy this, we use both active and passive infrared methods together. In addition to the mean surface renewal time obtained from the decay rate of the active heat markers, we calculate the two-dimensional surface velocity  $\mathbf{u}$  and other kinematic variables from infrared surface temperature images (Veron et al. 2008a). The velocity at the surface can further be projected onto the directions parallel and perpendicular to the wind or wave directions. Here, we employ an algorithm typically employed for particle image velocimetry and calculate the surface velocity by performing a running normalized cross correlation on subwindows of surface temperature images separated by 33 ms. Each cross correlation yields a local average displacement (over the subwindow) that is then used in conjunction with the instantaneous image resolution and time interval between the successive images to estimate an average surface horizontal velocity. In most cases, we used 8 pixel  $\times$  8 pixel subimages with 50% linear overlap and image pairs separated by 166 ms yielding six velocity maps per second, each having a spatial resolution of approximately 3 cm. From the velocity field, the first-order derivatives and the velocity gradient tensor are readily obtained. Details on the performance of this technique can be found in Veron et al. (2008a). In the following, we explore the possibility of using results from these passive infrared techniques to aid in finding appropriate scaling variables. As we have seen from Fig. 7 and Eq. (21), the use of the shear production term in the Komogorov-type scaling is likely to be limited in validity because turbulence is not necessarily always shear generated. A more judicious approach might be to directly use surface turbulence parameters. One choice that would seem physical would be to use the divergence of the surface velocity field (see, e.g., the surface divergence models of Turney et al. 2005). Going back to

Eq. (21) and replacing the mean shear frequency  $\partial\bar{U}/\partial z$  by the rms surface divergence,

$$\delta = \sqrt{(\mathbf{V} \cdot \mathbf{u})^2}, \quad (24)$$

where  $\mathbf{u}$  is the horizontal velocity vector, we define the following time scale:

$$t_\delta = \left( \frac{u_w^2 \delta}{\nu_w} \right)^{-1/2}. \quad (25)$$

Figure 8 shows the measured mean surface renewal time  $t_*$  as a function of  $t_\delta$ . The agreement is remarkable and robust over the full range of conditions studied. The solid line shown has a slope of one. A linear fit through the whole dataset yields a slope of 1.08 with  $r^2 = 0.93$ . The use of the measured surface turbulence parameters appears to unify the complete dataset over the whole range of conditions studied here. This indicates that various measures of surface turbulence might, indeed, be more appropriate descriptors of the surface renewal events rather than proxies such as wind speeds and other boundary layer scaling parameters. We suggest that these measures of surface turbulence should be favored in the development of surface renewal parameterizations. Results such as those shown in Fig. 8, along with the analysis presented in section 3, point toward the possibility of measuring the air–sea heat flux using the surface renewal framework.

### b. Surface heat flux estimates

To estimate the heat flux from the surface renewal approach, one needs to evaluate Eq. (19) and solve for the heat flux  $Q$ . From the passive infrared imagery presented in the previous section, we obtain  $\Delta T_0$  (Fig. 5), while the active infrared technique gives a direct measurement of the mean renewal time  $t_* = \int_0^\infty \tau \Pi(\tau) d\tau$  in which  $\Pi(\tau)$  is the surface-age distribution function. Unfortunately, the CFT technique only yields the mean renewal time, and some assumptions must be made with regard to the complete PDF of the surface renewal time scales. Historically, an exponential distribution function was adopted (Danckwerts 1951), but other probability density functions have been proposed (Garbe et al. 2004; Atmane et al. 2004). Here, we find that the best comparison between modeled and measured heat fluxes is obtained using a  $\chi$  distribution (chi distribution) where

$$\Pi(\tau) = \chi(\tau) = \frac{\tau^{q-1} e^{-\tau/2}}{2^{(q/2-1)} \Gamma(q/2)}. \quad (26)$$

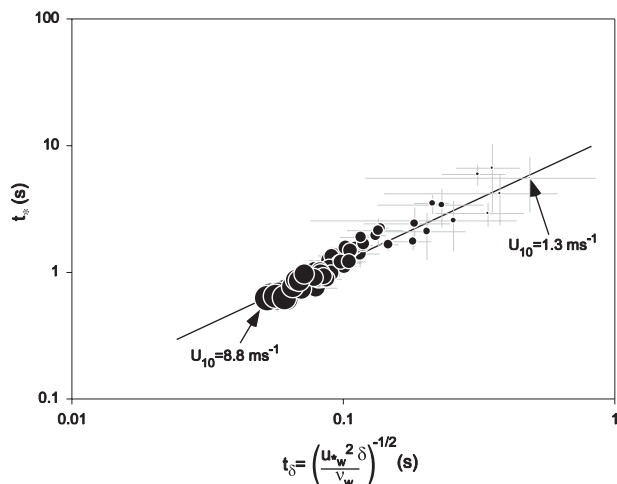


FIG. 8. Mean surface renewal time  $t_*$  as a function of the turbulent time scale  $t_\delta$  using the rms surface divergence  $\delta$ . The diameter of the symbols is proportional to the wind speed. The solid line has a slope of 1.

From the measurements of  $t_*$  obtained from the decay rate of the active heat markers, Eq. (5), we estimate the order  $q$  of the  $\chi$  distribution:

$$\begin{aligned} t_* &= \int_0^\infty \tau \chi(\tau) d\tau \\ &= \frac{\sqrt{2} \Gamma(q/2 + 1/2)}{\Gamma(q/2)}. \end{aligned} \quad (27)$$

Once  $q$  is determined, we simply solve Eq. (19) and find that

$$Q = \frac{\Delta T_0 \rho C_p \sqrt{\pi \kappa} \Gamma(q/2)}{2^{5/4} \Gamma(1/4 + q/2)}. \quad (28)$$

Figure 9a shows, as a function of  $U_{10}$ , the values of  $q$  obtained from the measured mean surface renewal time  $t_*$  using Eq. (27). The panel shows a similar behavior as that shown on Fig. 7, which is simply a consequence of the monotonic character of Eq. (27). Also, Fig. 9b shows examples of the  $\chi$  distribution for different orders  $q$ , corresponding to a representative range of wind speeds for our dataset. We note here that a  $\chi$  distribution on the order of  $q \leq 1$  (found here for wind speeds higher than  $\sim 6\text{--}7 \text{ m s}^{-1}$ ) has a shape similar to an exponential distribution, that is, it is unbounded for small renewal times, whereas the  $\chi$  distribution for  $q \geq 1$ , although more symmetrical, adopts a shape comparable to that of a lognormal distribution, similar to that of Garbe et al. (2004).

Figure 10 shows the estimate of the heat flux obtained from the controlled flux technique  $Q_{\text{cft}}$  [Eq. (28)],

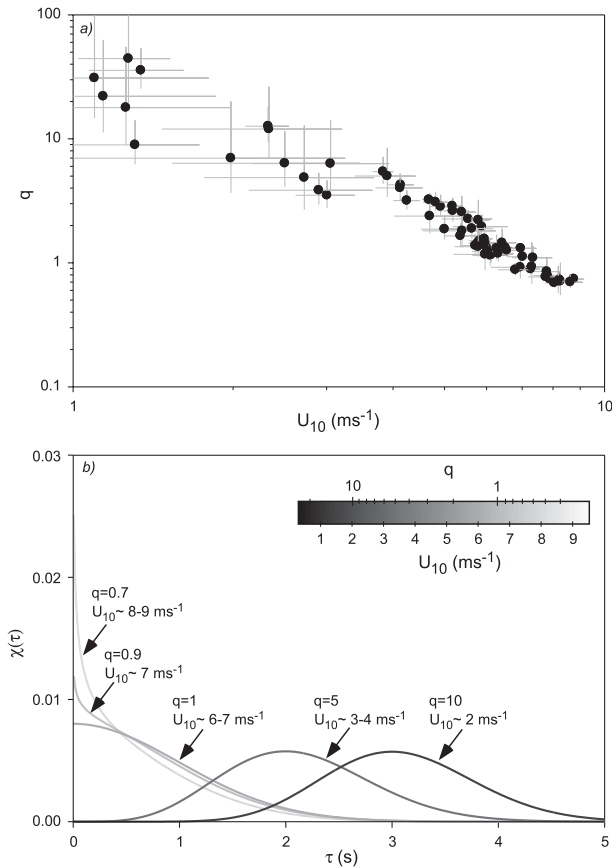


FIG. 9. (a) Estimate of the order  $q$  of the  $\chi$  distribution as a function of wind speed. (b) Several examples of the functional shape of the  $\chi$  distribution for multiple  $q$  corresponding to a wide range of wind speeds.

compared with the net heat flux  $Q_{\text{net}}$  measured with the meteorological package. The solid line shows the one-to-one correspondence. The agreement is acceptable and the estimate of the net heat flux from the CFT is within a factor of 2 of the net heat flux measured directly. This is in contrast to the measurements of Asher et al. (2004), who found that their CFT measurements overestimated the heat flux by up to a factor of 7. Although the agreement found here is satisfactory, especially at the higher heat fluxes, it appears that the low heat flux regime (less than about  $100 \text{ W m}^{-2}$ ) exhibits larger errors. Other surface-age distribution functions might lead to similar results. For instance, we find that surface-age distributions with surface renewal times distributed like powers of a  $\chi$  distribution between  $\chi$  and  $\chi^2$ , such as  $\chi^{3/2}$ , or a Maxwell–Boltzmann distribution lead to similarly acceptable results overall, with improved agreement in the low heat flux regime. However, over the full dataset, the mean error is not significantly improved, and it is not possible to unequivocally determine a single

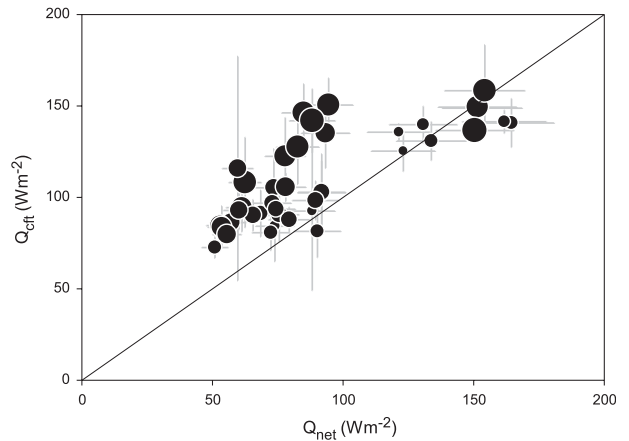


FIG. 10. Estimate of the heat flux obtained from the controlled flux technique,  $Q_{\text{cft}}$  from Eq. (28), compared with the net heat flux  $Q_{\text{net}}$  measured with the eddy covariance system. The diameter of the symbols is proportional to the wind speed and the solid line shows the one-to-one correspondence.

surface-age distribution function that is universally satisfactory. It is conceivable, and perhaps likely, that not one distribution can be used to represent a wide range of forcing conditions and turbulent regimes. Furthermore, it has also been suggested that, rather than having a temporal distribution of surface renewal events, these might instead be distributed in space with turbulent eddies possibly renewing the surface layer only partially (Atmane et al. 2004; Jessup et al. 2009). Regardless of the surface-age PDF, a crucial parameter, which in fact appears to be the main source of the difference between the results presented here and that of Asher et al. (2004), is the value of  $\Delta T_0$  used in Eq. (19).

### 5. Conclusions

We have shown that the surface renewal theory originally presented by Higbie (1935) and later applied by Danckwerts (1951) for gas transfer applications was perhaps hastily applied to the heat transfer problem. Indeed, while the basic physics of these scalar transfers through the molecular diffusive surface layers are identical, we showed that the difference in surface boundary conditions for heat and gas, namely constant flux and constant concentration difference, respectively, lead to vastly different solutions to the simple diffusion problem. However, within the surface renewal framework, the relationship between skin – subskin temperature difference and surface heat flux (i.e., the Fickian diffusion law) is identical for both surface conditions if the PDF of the surface renewal times is strictly given by

an exponential distribution. This PDF is widely used in the, so-called, controlled-flux technique that uses active surface thermal markers to directly estimate the mean surface renewal rates. Therefore, previous estimates of heat fluxes made with the CFT technique are not in error provided that the PDF of surface renewal times is, indeed, exponential. We note here that the active CFT technique gives an estimate of the mean surface renewal rate, which is the first moment of the exponential distribution, but does not measure the PDF itself. In fact, recent work (Garbe et al. 2004; Atmane et al. 2004), including the results presented in this paper, suggests that other PDFs might also be appropriate. The  $\chi$  distribution leads to an accurate description of the skin – subskin temperature difference, and we show that it leads to a reasonable estimate of the surface heat flux. If surface renewal time scales are better described by PDFs other than exponential, then the different solutions to the diffusion problem for heat and gas (for different boundary conditions) cast doubts on the use of heat as a proxy for surface gas transfer estimates. This is separate from the fact that air–sea surface heat transfer can never account for the contribution of bubble entrainment to gas transfer. Finally, we showed that, at moderate wind speeds, the surface renewal time scale compares favorably with the rate of ejection of a turbulent burst from turbulent boundary layers over flat solid surfaces, provided that the outer scaling involves a nearly constant boundary layer depth. At low wind speeds, it is likely that turbulent convection dominates, whereas over the intermediate wind speeds the shear generation of turbulence might be more significantly affected by breaking surface waves and Langmuir circulations. Finally, we have shown that the surface renewal rate scales very well with surface turbulent parameters over the whole range of slow and intermediate wind speeds studied here. In particular, when using the rms surface divergence, we derived a time scale that predicts the measured surface renewal time scale robustly and independently of the turbulence generation mechanisms. We conclude that the direct use of surface turbulence measurements will be a more productive approach for studying and better understanding air–sea scalar fluxes.

*Acknowledgments.* We thank Peter Matusov for his help in the design, construction, testing, and deployment of the original instrumentation. We thank Bill Gaines and the captain and crew of the R/P *FLIP* for all their help in the field experiments. We thank John Hildebrand and Gerald D’Spain for sharing space and facilities on *FLIP*. This research was supported by an NSF grant (OCE 01-18449) to WKM and FV and an ONR (Physical Oceanography) grant to WKM.

## REFERENCES

- Agrawal, Y., E. Terray, M. A. Donelan, P. Hwang, A. J. Williams III, W. M. Drennan, K. K. Kahma, and S. A. Kitaigorodskii, 1992: Enhanced dissipation of kinetic energy beneath surface waves. *Nature*, **359**, 219–220.
- Andreas, E. L., 2004: Spray stress revisited. *J. Phys. Oceanogr.*, **34**, 1429–1440.
- Anis, A., and J. N. Moum, 1995: Surface wave–turbulence interactions: Scaling  $\epsilon(z)$  near the sea surface. *J. Phys. Oceanogr.*, **25**, 2025–2045.
- Asher, W. E., and J. F. Pankow, 1989: Direct observations of concentration fluctuations close to a gas–liquid interface. *Chem. Eng. Sci.*, **44**, 1451–1455.
- , A. T. Jessup, and M. A. Atmane, 2004: Oceanic application of the active controlled flux technique for measuring air–sea transfer velocities of heat and gases. *J. Geophys. Res.*, **109**, C08S12, doi:10.1029/2003JC001862.
- Atmane, M. A., W. E. Asher, and A. T. Jessup, 2004: On the use of the active infrared technique to infer heat and gas transfer velocities at the air–water free surface. *J. Geophys. Res.*, **109**, C08S14, doi:10.1029/2003JC001805.
- Brutsaert, W., 1975: A theory for local evaporation (or heat transfer) from rough and smooth surfaces at ground level. *Water Resour. Res.*, **11**, 543–550.
- Businger, J. A., J. C. Wyngaard, Y. Izumi, and E. F. Bradley, 1971: Flux–profile relationships in the atmospheric surface layer. *J. Atmos. Sci.*, **28**, 181–189.
- Castro, S. L., G. A. Wick, and W. J. Emery, 2003: Further refinements to models for the bulk–skin sea surface temperature difference. *J. Geophys. Res.*, **108**, 3377, doi:10.1029/2002JC001641.
- Clayson, C. A., C. W. Fairall, and J. A. Curry, 1996: Evaluation of turbulent fluxes at the ocean surface using surface renewal theory. *J. Geophys. Res.*, **101**, 28 503–28 513.
- Danckwerts, P. V., 1951: Significance of liquid–film coefficients in gas absorption. *Ind. Eng. Chem.*, **43**, 1460–1467.
- Donelan, M. A., B. K. Haus, N. Reul, W. J. Plant, M. Stiassnie, H. C. Graber, O. B. Brown, and E. S. Saltzman, 2004: On the limiting aerodynamics roughness on the ocean in very strong winds. *Geophys. Res. Lett.*, **31**, L18306, doi:10.1029/2004GL019460.
- Donlon, C. J., and I. S. Robinson, 1997: Observations of the oceanic thermal skin in the Atlantic Ocean. *J. Geophys. Res.*, **102**, 18 585–18 606.
- , W. Eifler, and T. J. Nightingale, 1999: The thermal skin temperature of the ocean at high wind speed. *Proc. Int. Geoscience and Remote Sensing Symposium (IGARSS)*, Hamburg, Germany, IEEE, Vol. 1, 8–10.
- , P. J. Minnett, C. Gentemann, T. J. Nightingale, I. J. Barton, B. Ward, and M. J. Murray, 2002: Toward improved validation of satellite sea surface skin temperature measurements for climate research. *J. Climate*, **15**, 353–369.
- Downing, H. D., and D. Williams, 1975: Optical constant of water in the infrared. *J. Geophys. Res.*, **80**, 1656–1661.
- Drennan, W. M., M. A. Donelan, E. A. Terray, and K. B. Katsaros, 1996: Oceanic turbulence dissipation measurements in SWADE. *J. Phys. Oceanogr.*, **26**, 808–815.
- Edson, J. B., C. J. Zappa, J. A. Ware, W. R. McGillis, and J. E. Hare, 2004: Scalar flux profile relationships over the open ocean. *J. Geophys. Res.*, **109**, C08S09, doi:10.1029/2003JC001960.
- Ewing, G., and E. D. McAlister, 1960: On the thermal boundary layer of the ocean. *Science*, **131**, 1374–1376.

- Fairall, C. W., E. F. Bradley, D. P. Rogers, J. B. Edson, and G. S. Young, 1996: Bulk parameterization of air-sea fluxes for Tropical Ocean-Global Atmosphere Coupled-Ocean Atmosphere Response Experiment. *J. Geophys. Res.*, **101**, 3747–3764.
- , —, J. E. Hare, A. A. Grachev, and J. B. Edson, 2003: Bulk parameterization of air-sea fluxes: Updates and verification for the COARE algorithm. *J. Climate*, **16**, 571–591.
- Farmer, D. M., C. L. McNeil, and B. D. Johnson, 1993: Evidence for the importance of bubbles in increasing air-sea gas flux. *Nature*, **361**, 620–623.
- Frew, N. M., and Coauthors, 2004: Air-sea gas transfer: Its dependence on wind stress, small-scale roughness, and surface films. *J. Geophys. Res.*, **109**, C08S17, doi:10.1029/2003JC002131.
- Garbe, C. S., U. Schimpf, and B. Jähne, 2004: A surface renewal model to analyze infrared image sequences of the ocean surface for the study of air-sea heat and gas exchange. *J. Geophys. Res.*, **109**, C08S15, doi:10.1029/2003JC001802.
- Gemmrich, J., and D. Farmer, 2004: Near-surface turbulence in the presence of breaking waves. *J. Phys. Oceanogr.*, **34**, 1067–1086.
- Hara, T., and S. E. Belcher, 2002: Wind forcing in the equilibrium range of wind-wave spectra. *J. Fluid Mech.*, **470**, 223–245.
- Haußecker, H., 1996: Messung und simulation von kleinskaligen austauschvorgängen an der ozeanoberfläche mittels thermographie. Ph.D. dissertation, University of Heidelberg, 197 pp.
- , S. Reinelt, and B. Jähne, 1995: Heat as a proxy tracer for gas exchange measurements in the field: Principles and technical realization. *Air-Water Gas Transfer*, B. Jähne and E. C. Monahan, Eds., Aeon-Verlag, 405–413.
- , U. Schimpf, C. S. Garbe, and B. Jähne, 2001: Physics from IR image sequences: Quantitative analysis of transport models and parameters of air-sea gas transfer. *Gas Transfer at Water Surfaces, Geophys. Monogr.*, Vol. 127, Amer. Geophys. Union, 103–108.
- Higbie, R., 1935: The rate of absorption of a pure gas into a still liquid during short periods of exposure. *Trans. Amer. Inst. Chem. Eng.*, **31**, 365–389.
- Ho, D. T., F. Veron, E. Harrison, L. F. Bliven, N. Scott, and W. R. McGillis, 2007: The combined effect of rain and wind on air-water gas exchange: A feasibility study. *J. Mar. Syst.*, **66** (1–4), 150–160.
- Hsu, C.-T., E. Y. Hsu, and R. L. Street, 1981: On the structure of turbulent flow over a progressive water wave: Theory and experiment in a transformed, wave-following co-ordinate system. *J. Fluid Mech.*, **105**, 87–117.
- Jähne, B., and H. Haußecker, 1998: Air-water gas exchange. *Annu. Rev. Fluid Mech.*, **30**, 443–468.
- , P. Libner, R. Fisher, T. Billen, and E. J. Plate, 1989: Investigating the transfer processes across the free aqueous viscous boundary layer by the controlled flux method. *Tellus*, **41**, 177–195.
- Jessup, A. T., C. J. Zappa, M. R. Loewen, and V. Hesany, 1997a: Infrared remote sensing of breaking waves. *Nature*, **385**, 52–55.
- , —, and J. H. Yeh, 1997b: Defining and quantifying microscale breaking with infrared imagery. *J. Geophys. Res.*, **102**, 23 145–23 153.
- , W. E. Asher, M. Atmane, K. Phadnis, C. J. Zappa, and M. R. Loewen, 2009: Evidence for complete and partial surface renewal at an air-water interface. *Geophys. Res. Lett.*, **36**, L16601, doi:10.1029/2009GL038986.
- Katsaros, K. B., 1980: The aqueous thermal boundary layer. *Bound.-Layer Meteor.*, **18**, 107–127.
- Kim, H. T., S. J. Kline, and W. C. Reynolds, 1971: The production of turbulence near smooth wall in a turbulent boundary layer. *J. Fluid Mech.*, **50**, 133–160.
- Kitaigorodskii, S. A., 1984: On the fluid dynamical theory of turbulent gas transfer across an air-sea interface in the presence of breaking wind-waves. *J. Phys. Oceanogr.*, **14**, 960–972.
- Komen, G. J., L. Cavaleri, M. Donelan, K. Hasselmann, S. Hasselmann, and P. A. E. M. Janssen, 1994: *Dynamics and Modelling of Ocean Waves*. Cambridge University Press, 532 pp.
- Kraus, E. B., and J. A. Businger, 1994: *Atmosphere-Ocean Interaction*. Oxford University Press, 362 pp.
- Kudryavtsev, V. N., and V. K. Makin, 2001: The impact of air-flow separation on the drag of the sea surface. *Bound.-Layer Meteor.*, **98**, 155–171.
- Liu, W. T., K. B. Katsaros, and J. A. Businger, 1979: Bulk parameterization of the air-sea exchange of heat and water vapor including the molecular constraints at the interface. *J. Atmos. Sci.*, **36**, 1722–1735.
- Luchik, T., and W. G. Tiederman, 1987: Timescale and structure of ejections and bursts in turbulent channel flows. *J. Fluid Mech.*, **174**, 529–552.
- McAlister, E. D., 1964: Infrared optical techniques applied to oceanography I. Measurement of total heat flow from the sea surface. *Appl. Opt.*, **5**, 609–612.
- , and W. McLeish, 1970: A radiometric system for airborne measurement of the total heat flow from the sea. *Appl. Opt.*, **9**, 2607–2705.
- Melville, W. K., 1994: Energy dissipation by breaking waves. *J. Phys. Oceanogr.*, **24**, 2041–2049.
- , 1996: The role of surface-wave breaking in air-sea interaction. *Annu. Rev. Fluid Mech.*, **28**, 279–321.
- , R. Shear, and F. Veron, 1998: Laboratory measurements of the generation and evolution of Langmuir circulations. *J. Fluid Mech.*, **364**, 31–58.
- , F. Veron, and C. J. White, 2002: The velocity field under breaking waves: Coherent structures and turbulence. *J. Fluid Mech.*, **454**, 203–233.
- Mueller, J. A., and F. Veron, 2009a: Nonlinear formulation of the bulk surface stress over breaking waves: Feedback mechanisms from air-flow separation. *Bound.-Layer Meteor.*, **130**, 117–134.
- , and —, 2009b: A sea state-dependent spume generation function. *J. Phys. Oceanogr.*, **39**, 2363–2372.
- Panofsky, H. A., and J. A. Dutton, 1984: *Atmospheric Turbulence: Models and Methods for Engineering Applications*. John Wiley, 397 pp.
- Paulson, C. A., and J. J. Simpson, 1981: The temperature difference across the cool skin of the ocean. *J. Geophys. Res.*, **86** (C11), 11 044–11 054.
- Rapp, R. J., and W. K. Melville, 1990: Laboratory measurements of deep-water breaking waves. *Philos. Trans. Roy. Soc. London*, **331A**, 735–800.
- Saunders, P. M., 1967: The temperature of the ocean-air interface. *J. Atmos. Sci.*, **24**, 269–273.
- Schimpf, U., C. Garbe, and B. Jähne, 2004: Investigation of transport processes across the sea surface microlayer by infrared imagery. *J. Geophys. Res.*, **109**, C08S13, doi:10.1029/2003JC001803.
- Schlüssel, P., W. J. Emery, H. Grassl, and T. Mammen, 1990: On the bulk-skin temperature difference and its impact on satellite remote sensing of the sea surface temperature. *J. Geophys. Res.*, **95**, 13 341–13 356.

- Snyder, R. L., F. W. Dobson, J. A. Elliott, and R. B. Long, 1981: Array measurements of atmospheric pressure fluctuations above surface gravity waves. *J. Fluid Mech.*, **102**, 1–59.
- Soloviev, A. V., and P. Schlüssel, 1994: Parameterization of the cool skin of the ocean and the air–ocean gas transfer on the basis of modeling surface renewal. *J. Phys. Oceanogr.*, **24**, 1339–1346.
- Sullivan, P. P., and J. C. McWilliams, 2002: Turbulent flow over water waves in the presence of stratification. *Phys. Fluids*, **14**, 1182–1195.
- , —, and C.-H. Moeng, 2000: Simulation of turbulent flow over idealized water waves. *J. Fluid Mech.*, **404**, 47–85.
- , —, and W. K. Melville, 2004: The oceanic boundary layer driven by wave breaking with stochastic variability. Part I: Direct numerical simulations. *J. Fluid Mech.*, **507**, 143–174.
- , —, and —, 2007: Surface gravity wave effects in the oceanic boundary layer: Large-eddy simulation with vortex force and stochastic breakers. *J. Fluid Mech.*, **593**, 405–452.
- Teixeira, M. A. C., and S. E. Belcher, 2002: On the distortion of turbulence by a progressive surface wave. *J. Fluid Mech.*, **458**, 229–267.
- Terray, E., M. A. Donelan, Y. Agrawal, W. M. Drennan, K. K. Kahma, A. J. Williams III, P. Hwang, and S. A. Kitaigorodskii, 1996: Estimates of kinetic energy dissipation under breaking waves. *J. Phys. Oceanogr.*, **26**, 792–807.
- Thorpe, S. A., 1993: Energy loss by breaking waves. *J. Phys. Oceanogr.*, **23**, 2498–2502.
- , T. R. Osborn, D. M. Farmer, and S. Vagle, 2003: Bubble clouds and Langmuir circulation: Observations and models. *J. Phys. Oceanogr.*, **33**, 2013–2031.
- Turney, D. E., W. C. Smith, and S. Banerjee, 2005: A measure of near-surface fluid motions that predicts air–water gas in a wide range of conditions. *Geophys. Res. Lett.*, **32**, L04607, doi:10.1029/2004GL021671.
- Veron, F., and W. K. Melville, 1999: Pulse-to-pulse coherent Doppler measurements of waves and turbulence. *J. Atmos. Oceanic Technol.*, **16**, 1580–1597.
- , and —, 2001: Experiments on the stability and transition of wind-driven water surfaces. *J. Fluid Mech.*, **446**, 25–65.
- , G. Saxena, and S. K. Misra, 2007: Measurements of the viscous tangential stress in the airflow above wind waves. *Geophys. Res. Lett.*, **34**, L19603, doi:10.1029/2007GL031242.
- , W. K. Melville, and L. Lenain, 2008a: Infrared techniques for measuring ocean surface processes. *J. Atmos. Oceanic Technol.*, **25**, 307–326.
- , —, and —, 2008b: Wave-coherent air–sea heat flux. *J. Phys. Oceanogr.*, **38**, 788–802.
- , —, and —, 2009: Measurements of ocean surface turbulence and wave–turbulence interactions. *J. Phys. Oceanogr.*, **39**, 2310–2323.
- Ward, B., 2006: Near-surface ocean temperature. *J. Geophys. Res.*, **111**, C02004, doi:10.1029/2004JC002689.
- , and M. A. Donelan, 2006: Thermometric measurements of the molecular sublayer at the air–water interface. *Geophys. Res. Lett.*, **33**, L07605, doi:10.1029/2005GL024769.
- Webb, E. K., G. I. Pearman, and R. Leuning, 1980: Measurements for density effects due to heat and water vapor transfer. *Quart. J. Roy. Meteor. Soc.*, **106**, 85–106.
- Wick, G. A., 1995: Evaluation of the variability and predictability of the bulk–skin SST difference with application to satellite-measured SST. Ph.D. dissertation, University of Colorado, 146 pp.
- , W. J. Emery, and P. Schlüssel, 1992: A comprehensive comparison between satellite-measured skin and multichannel sea surface temperature. *J. Geophys. Res.*, **97** (C4), 5569–5595.
- , —, L. H. Kantha, and P. Schlüssel, 1996: The behavior of the bulk – skin sea surface temperature difference under varying wind speed and heat flux. *J. Phys. Oceanogr.*, **26**, 1969–1988.
- , J. C. Ohlmann, C. W. Fairall, and A. T. Jessup, 2005: Improved oceanic cool-skin corrections using a refined solar penetration model. *J. Phys. Oceanogr.*, **35**, 1986–1996.
- Zappa, C. J., W. E. Asher, and A. T. Jessup, 2001: Microscale wave breaking and air–water gas transfer. *J. Geophys. Res.*, **106** (C5), 9385–9391.

## CORRIGENDUM

FABRICE VERON

*School of Marine Science and Policy, University of Delaware, Newark, Delaware*

W. KENDALL MELVILLE AND LUC LENAIN

*Scripps Institution of Oceanography, University of California, San Diego, La Jolla, California*

---

Because of a production error in Veron et al. (2011), Eq. (9) was incorrect. The correct equation is as follows:

$$Q(t) = \sum_i \alpha_i t^i. \quad (9)$$

AMS and the staff of the *Journal of Physical Oceanography* regret any inconvenience this error may have caused.

### REFERENCE

Veron, F., W. K. Melville, and L. Lenain, 2011: The effects of small-scale turbulence on air–sea heat flux. *J. Phys. Oceanogr.*, **41**, 205–220.

---

*Corresponding author address:* Fabrice Veron, 112C Robinson Hall. University of Delaware, School of Marine Science and Policy, College of Earth, Ocean and Environment, Newark, DE 19716.  
E-mail: fveron@udel.edu